THE JOURNAL OF PHYSICAL CHEMISTRY C

ARTICLE

pubs.acs.org/JPCC

Heterojunction Organic Photovoltaic Cells as Molecular Heat Engines: A Simple Model for the Performance Analysis

Mario Einax,*[,†,‡] Marcel Dierl,[†] and Abraham Nitzan*[,‡]

[†]Fachbereich Physik, Universität Osnabrück, Barbarastrasse 7, 49076 Osnabrück, Germany

[‡]School of Chemistry, Tel Aviv University, Tel Aviv 69978, Israel

ABSTRACT: Organic heterojunction solar cells are analyzed within a minimal model that includes the essential physical features of such systems. The dynamical properties of this model, calculated using a master equation approach, account for the qualitative behavior of such systems. The model yields explicit results for current−voltage behavior as well as performance characteristics expressed in terms of the thermodynamic efficiency as well as the power conversion efficiency at maximum power, making it possible to evaluate the optimal setup for this device model.

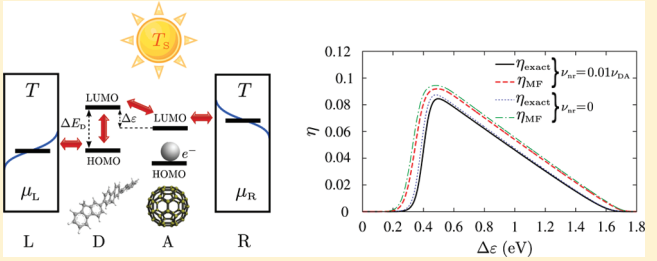

INTRODUCTION

The limited supply of today's main energy sources, such as oil and coal, will force us to rely increasingly on renewable energy sources. Besides wind and water power, energy conversion based on photovoltaic (PV) devices has received much attention as such a source. Promising systems for next generation devices are organic photovoltaic solar cells (OPV) because of their potential for low-cost processing. Of particular interest are polymer-based heterojunctions consisting of a blend of electron-donor (D) and electron-acceptor (A) material. (For reviews, see refs 1 and 2 and references therein.) A prominent acceptor material is the buckminsterfullerene (C_{60}).[3−6] The quest to improve the energy conversion efficiency of such systems is the focus of intensive current research.

To evaluate and subsequently improve the efficiency of OPV cells, it is crucial to understand the underlying energy conversion processes and how material properties affect their overall performance. Widely accepted is the multistep generation process that starts with photon absorption by the donor (often a polymer) yielding an exciton (bounded electron−hole pair). The generated exciton diffuses to the D−A interface, where it dissociates into free charge carriers, which are later transported to the electrodes. The D−A interface should be constructed to favor energetically fast and efficient electron transfer leading to exciton dissociation.

The dynamics of electron transfer at the D−A interface is of crucial importance for the performance of heterojunction solar cells, as measured by their efficiency. In considering this issue, one may address the thermodynamic efficiency η^*[7,8] by considering the solar cell as a heat engine operating between a hot and a cold reservoir with temperatures T_S ("sun temperature", representing the incident radiation) and T (temperature of the chemical environment), respectively. Alternatively, the conversion efficiency η[9] associated with the maximum power point in the current−voltage ($J-U$) characteristic is of interest as a realistic performance measure. Establishing the relationship between system properties that affect exciton dissociation at the D−A interface and the cell efficiency is a major goal of the ongoing research. Within this effort, it is useful to consider simple model systems for which one can obtain explicit relationships between system structure and characteristic parameters and its performance measures. In this Article, we describe and analyze such a model system.

Our model consists of coupled donor and acceptor molecules, each described as a two-level (highest occupied molecular level, HOMO, and lowest unoccupied molecular level, LUMO) system, situated between two electrodes. As such, it is an extension of a simpler model recently analyzed in a similar context by Rutten et al.[7] but with an important additional feature − the existence of an heterojunction characterized by energetic parameters − Coulomb interaction and donor−acceptor LUMO−LUMO gap, which were identified as important driving factors in the operation of such systems. The system dynamics associated with this model is described by a kinetics scheme derived using a lattice gas approach,[10−12] similar in spirit to previous work[13−17] that uses a master equation approach to analyze cell dynamics.

We show that an effective mechanism for both exciton pair formation and dissociation can be captured by a minimal model of this type, which can be used as a framework for discussing the current− and power−voltage curves and the cell efficiency. In particular, the model leads directly to the predictions of an optimal interface energy gap $\Delta\varepsilon$ (usually associated with the energy difference between the lowest unoccupied molecular levels (LUMOs) of the D and A molecules) for these efficiency measures. This can be compared with the performance of an ideal device, in which nonradiative losses are absent. In this ideal case,

Received: June 22, 2011
Revised: September 8, 2011
Published: September 15, 2011

dx.doi.org/10.1021/jp205856x | *J. Phys. Chem. C* 2011, 115, 21396–21401

Table 1. System States and Their Occupations with Corresponding Energies

state	occupation $(n_{D1},n_{D2},n_{A1},n_{A2})$	energy
0	(0,0,1,0)	$\varepsilon_0 = \varepsilon_{A1}$
1	(1,0,1,0)	$\varepsilon_1 = \varepsilon_{D1} + \varepsilon_{A1}$
2	(0,1,1,0)	$\varepsilon_2 = \varepsilon_{D2} + \varepsilon_{A1}$
3	(0,0,1,1)	$\varepsilon_3 = \varepsilon_{A1} + \varepsilon_{A2} + V_C + V_C' = \varepsilon_{A1} + \tilde{\varepsilon}_{A2} + V_C'$
4	(1,0,1,1)	$\varepsilon_4 = \varepsilon_{D1} + \varepsilon_{A1} + \varepsilon_{A2} + V_C = \varepsilon_{D1} + \varepsilon_{A1} + \tilde{\varepsilon}_{A2}$
5	(0,1,1,1)	$\varepsilon_5 = \varepsilon_{D2} + \varepsilon_{A1} + \varepsilon_{A2} + V_C = \varepsilon_{D2} + \varepsilon_{A1} + \tilde{\varepsilon}_{A2}$

the thermodynamic efficiency is found to decrease monotonously, whereas the power conversion efficiency still goes through a maximum, with increasing $\Delta\varepsilon$.

MODEL AND COMPUTATIONAL DETAILS

Model. The PV cell model considered here is a 1D lattice gas with two "effective" sites l = D, A. One site represents the donor (D, e.g., polymer-based material) and the second acts as acceptor (A, e.g., fullerene-based material). Each of the sites is represented as a two-state system with energy levels $(\varepsilon_{D1},\varepsilon_{D2})$ and $(\varepsilon_{A1},\varepsilon_{A2})$ corresponding to the (HOMO, LUMO) levels of the donor and acceptor species, respectively. In what follows, we use the notation $\Delta E_l = \varepsilon_{l2} - \varepsilon_{l1}$ (l = D, A) for the energy differences that represent the donor and acceptor band gaps and refer to $\Delta\varepsilon = \varepsilon_{D2} - \varepsilon_{A2}$ as the interface or donor−acceptor LUMO−LUMO gap. The microstates of the system can be specified by the set of occupation numbers $n = (n_{D1},n_{D2},n_{A1},n_{A2})$, where $n_{lj} = 0$ or 1 ($l = D, A$; $j = 1,2$) if the corresponding level is vacant or occupied by an electron.

To assign further realistic contents to this model, we introduce the restrictions $n_{D1}n_{D2} = 0$ and $n_{A1} = 1$. The first of these restrictions implies that the donor can be in the ground or excited state, or, following charge separation, in positively ionized state but excludes its doubly occupied (negatively charged) state. The excited donor state $(n_{D1},n_{D2}) = (0,1)$ represents the exciton formed as result of light absorption. The second condition implies that the acceptor can be in either its ground $(n_{A1},n_{A2}) = (1,0)$ or its negative ion $(n_{A1},n_{A2}) = (1,1)$ states. Therefore, the system is characterized by six states with respect to the occupations $(n_{D1},n_{D2},n_{A1},n_{A2})$, that we denote by the integers 0, ..., 5 as shown in Table 1.

In the expressions for the states energies, $V_C > 0$ is the Coulombic repulsion between two electrons on the acceptor, whereas $V_C' > 0$ is the Coulombic energy cost to move an electron away from the hole remaining on the donor. In general, we expect that $V_C > V_C'$. The sum $V_C + V_C'$ can be thought of as the exciton binding energy in this model: It is the total Coulomb energy cost for dissociating the exciton on the donor by moving an electron to the acceptor. It is convenient to redefine $\tilde{\varepsilon}_{A2} = \varepsilon_{A2} + V_C$ so that the energies ε_j ($j = 0, ..., 5$) are determined by the five energy parameters ε_{D1}, ε_{D2}, ε_{A1}, $\tilde{\varepsilon}_{A2}$, and V_C'.

At the left (donor, say) and right (acceptor) ends of the system, the device is connected with two electrodes represented by free-electron reservoirs at chemical potentials μ_K (K = L, R). This is a highly simplified picture that disregards electron transport within the donor and acceptor phases. We have opted to make this simplification to focus on the important step of interfacial exciton dissociation, but future more realistic treatments should take these components of the overall dynamics into consideration. As sketched in Figure 1, we use the common picture by which the left reservoir is assumed to exchange electrons only with the HOMO level of the donor, whereas the right lead exchange electrons with the upper level of the acceptor. Direct electronic interaction between system and reservoirs is not explicitly taken into account, but it is implicit both in the states of molecular species adjacent to metal electrodes and in the kinetic charge transfer rates.

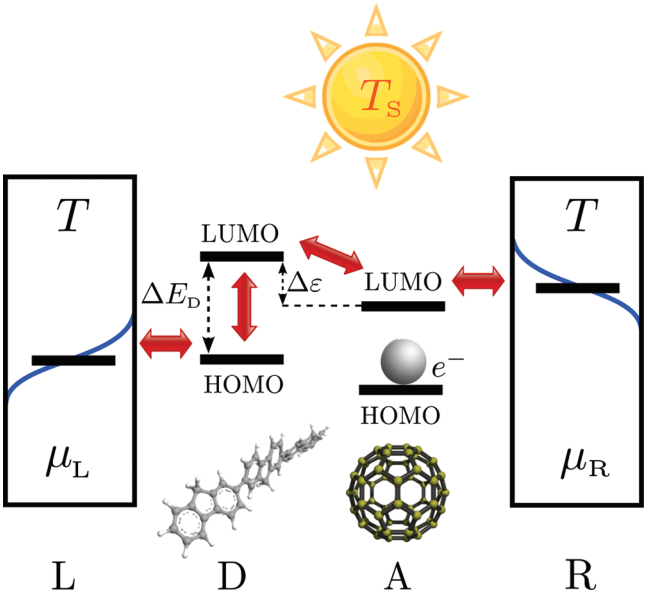

Figure 1. Minimal model of an organic heterojunction PV cell. The system consists of one donor (e.g., a suitable polymer) and one acceptor, for example, fullerene sites, each characterized by their HOMO and LUMO levels.

Next, we construct the kinetic scheme for the time evolution of the average occupations P_j ($j = 0, ..., 5$) associated with this level structure. (See Figure 2.) In writing these equations, we make the simplifying assumption that electron exchange between molecules and metals involve only metal electrons at the electrochemical potentials μ_L and μ_R of the left and right leads (corresponding to a bias potential $U = (\mu_R - \mu_L)/|e|$ where e is the electron charge). We also disregard possible environmental relaxation dynamics due to polarization effects associated with the formation of transient charged molecular species. Generalizing this dynamical picture to take such processes into account (e.g., by considering time-dependent site energies[18]) is another important subject for future work. The kinetics process in our scheme then corresponds to the following processes:

(a) Electron transfer between levels D1 and the left electrode and between A2 and the right electrode, with rates determined by the corresponding molecular energies, molecules-leads coupling, electrochemical potentials in the leads, and the environmental temperature, T.

(b) Electron transfer between donor and acceptor, determined by the coupling between them, the corresponding state energies, and the temperature, T.

dx.doi.org/10.1021/jp205856x |J. Phys. Chem. C 2011, 115, 21396–21401

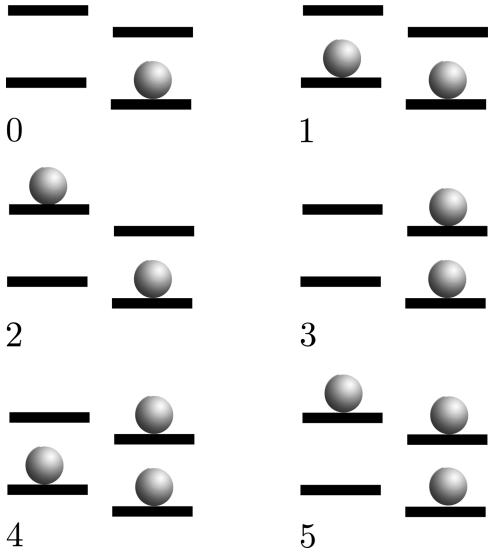

Figure 2. Six accessible microstates of the model system considered. The probability to find the system in state j (j = 0, ..., 5) is denoted P_j.

(c) Light-induced electron excitation (rate k_s) and relaxation (rate $\tilde{k}_s$) between donor levels D1 and D2. These rates are modeled as thermal rates determined by the corresponding state energies and radiative coupling, and the "sun temperature" T_s.

(d) Radiationless (thermal) electron transitions between level D1 and D2 with rates k_{nr} (excitation) and $\tilde{k}_{nr}$ (relaxation), determined as in (c) except that relevant coupling is vibronic in origin and the temperature involved is the environmental temperature T.

Explicitly, the transition rates $k_{j'j} = k_{j' \leftarrow j}$ from state j to j' are given by

$$k_{01} = k_{34} \equiv \tilde{k}_L = \nu_L \tilde{f}(x_L) \tag{1}$$

$$k_{10} = k_{43} \equiv k_L = \nu_L f(x_L) \tag{2}$$

$$\begin{aligned} k_{12} &= k_{45} \equiv \tilde{k}_S + \tilde{k}_{nr} \\ &= \nu_S(1 + n_S(x_S)) + \nu_{nr}(1 + n_{nr}(x_{nr})) \end{aligned} \tag{3}$$

$$k_{21} = k_{54} \equiv k_S + k_{nr} = \nu_S n_S(x_S) + \nu_{nr} n_{nr}(x_{nr}) \tag{4}$$

$$k_{32} \equiv \tilde{k}_{DA} = \nu_{DA} \tilde{f}(x_{DA}) \tag{5}$$

$$k_{23} \equiv k_{DA} = \nu_{DA} f(x_{DA}) \tag{6}$$

$$k_{03} = k_{14} = k_{25} \equiv \tilde{k}_R = \nu_R \tilde{f}(x_R) \tag{7}$$

$$k_{30} = k_{41} = k_{52} \equiv k_R = \nu_R f(x_R) \tag{8}$$

In these equations $f(x) = 1/[\exp(x) + 1]$ and $\tilde{f}(x) \equiv 1 - f(x)$, $x_L = (\varepsilon_{D1} - \mu_L)/k_B T$, $x_R = (\tilde{\varepsilon}_{A2} - \mu_R)/k_B T$, and $x_{DA} = (\varepsilon_{D2} - \tilde{\varepsilon}_{A2} - V_C')/k_B T$. The rate coefficients ν are determined by the corresponding couplings. Following ref 7, the transition rates between the HOMO and LUMO in the donor phase are assigned by using the boson population factors $n_s = 1/[\exp(x_s) - 1]$ and $n_{nr} = 1/[\exp(x_{nr}) - 1]$ with scaled energies $x_S = \Delta E_D/k_B T_S$ and $x_{nr} = \Delta E_D/k_B T$. $k_L \equiv k_{01} = k_{34}$ is the rate to move an electron from level D1 to the left electrode, $\tilde{k}_R \equiv k_{03} = k_{14} = k_{25}$ is similarly the rate from A2 to the right electrode. $k_L \equiv k_{10} = k_{43}$ and $k_R \equiv k_{30} = k_{41} = k_{52}$ are the corresponding reverse rates. The transition rate from D2 to A2 is given by $\tilde{k}_{DA} \equiv k_{32}$, whereas the opposite rate is $k_{DA} \equiv k_{23}$. Also, we denote by k_S and k_{nr} the radiative and thermal excitation rates in the donor and by $\tilde{k}_s$ and $\tilde{k}_{nr}$ the corresponding relaxation rates, so $k_S + k_{nr} \equiv k_{21} = k_{54}$ and $\tilde{k}_s + \tilde{k}_{nr} \equiv k_{12} = k_{45}$.

Computational Details. The master equation with the rates eqs 1−8 that describe the time evolution of the probabilities $P_j = P(n_{D1}, n_{D2}, n_{A1}, n_{A2})$ (j = 0, ..., 5) to be in the six possible states thus reads

$$\frac{dP_0(t)}{dt} = k_{01}P_1(t) + k_{03}P_3(t) - (k_{10} + k_{30})P_0(t) \tag{9}$$

$$\frac{dP_1(t)}{dt} = k_{10}P_0(t) + k_{14}P_4(t) + k_{12}P_2(t) - (k_{01} + k_{41} + k_{21})P_1(t) \tag{10}$$

$$\frac{dP_2(t)}{dt} = k_{21}P_1(t) + k_{23}P_3(t) + k_{25}P_5(t) - (k_{12} + k_{32} + k_{52})P_2(t) \tag{11}$$

$$\frac{dP_3(t)}{dt} = k_{30}P_0(t) + k_{32}P_2(t) + k_{34}P_4(t) - (k_{03} + k_{23} + k_{43})P_3(t) \tag{12}$$

$$\frac{dP_4(t)}{dt} = k_{43}P_3(t) + k_{41}P_1(t) + k_{45}P_5(t) - (k_{34} + k_{14} + k_{54})P_4(t) \tag{13}$$

and normalization implies that

$$P_5(t) = 1 - \sum_{j=0}^{4} P_j(t) \tag{14}$$

In terms of these probabilities electron currents can be expressed as

$$J_L(t) = k_L(P_0 + P_3) - \tilde{k}_L(P_1 + P_4) \tag{15}$$

$$J_R(t) = \tilde{k}_R(P_3 + P_4 + P_5) - k_R(P_0 + P_1 + P_2) \tag{16}$$

$$J_S(t) = k_S(P_1 + P_4) - \tilde{k}_S(P_2 + P_5) \tag{17}$$

$$J_{nr}(t) = k_{nr}(P_1 + P_4) - \tilde{k}_{nr}(P_2 + P_5) \tag{18}$$

$$J_{DA}(t) = \tilde{k}_{DA}P_2 - k_{DA}P_3 \tag{19}$$

J_L (J_R) is the current entering (leaving) the molecular system from (to) the electrodes, J_S and J_{nr} are, respectively, the light-induced and nonradiative transition currents between the HOMO and the LUMO in the donor phase, and J_{DA} is the average current between the donor and acceptor species. Below we will focus on the steady-state magnitude, $J_L = J_R = J_{DA} = J_S + J_{nr} = J$, of these currents.

The time evolution and steady-state currents associated with this kinetic model can be evaluated exactly; however, such exact solution becomes costly for a larger, more realistic system that takes into account also transport within the donor and acceptor

phases. We therefore advance also an approximate mean-field treatment and show that it can provide a good approximation to the exact analysis and can be used for realistic multilevel systems at a relatively low computational cost.

To this end, we introduce the averaged site occupations $p_{D1}(t) \equiv \langle n_{D1}\rangle = P_1(t) + P_4(t)$, $p_{D2}(t) \equiv \langle n_{D2}\rangle = P_2(t) + P_5(t)$, and $p_{A2}(t) \equiv \langle n_{A2}\rangle = P_3(t) + P_4(t) + P_5(t)$. (See also the illustration in Figure 2.) Therefore, the currents eqs 15−19 can be rewritten as follows

$$J_L(t) = k_L(\tilde{p}_{D1} - p_{D2}) - \tilde{k}_L p_{D1} \tag{20}$$

$$J_R(t) = \tilde{k}_R p_{A2} - k_R \tilde{p}_{A2} \tag{21}$$

$$J_S(t) = k_S p_{D1} - \tilde{k}_S p_{D2} \tag{22}$$

$$J_{nr}(t) = k_{nr} p_{D1} - \tilde{k}_{nr} p_{D2} \tag{23}$$

where $\tilde{p} = 1 - p$. The treatment of the average current $J_{DA}(t)$ between the donor and acceptor species is more difficult. In terms of occupation number, $J_{DA}(t)$ is

$$J_{DA}(t) = \tilde{k}_{DA}\langle n_{D2}(1 - n_{A2})\rangle - k_{DA}\langle(1 - n_{D1} - n_{D2})n_{A2}\rangle \tag{24}$$

Neglecting fluctuations, that is, $\langle n_{D1}n_{A2}\rangle \approx \langle n_{D1}\rangle\langle n_{A2}\rangle = p_{D1}p_{A2}$ and $\langle n_{D2}n_{A2}\rangle \approx \langle n_{D2}\rangle\langle n_{A2}\rangle = p_{D2}p_{A2}$, leads to the mean-field expression of the current

$$J_{DA}^{MF}(t) = \tilde{k}_{DA} p_{D2}\tilde{p}_{A2} - k_{DA}(\tilde{p}_{D1} - p_{D2})p_{A2} \tag{25}$$

As a consequence, we arrive at the following mean-field rate equations for the averaged site occupations

$$\frac{dp_{D1}}{dt} = J_L(t) - J_S(t) - J_{nr}(t) \tag{26}$$

$$\frac{dp_{D2}}{dt} = J_S(t) + J_{nr}(t) - J_{DA}^{MF}(t) \tag{27}$$

$$\frac{dp_{A2}}{dt} = J_{DA}^{MF}(t) - J_R(t) \tag{28}$$

The full kinetics in this approximation is obtained by solving eqs 26−28 together with eqs 20, 23, and 25 self-consistently. Note that the number of coupled equations solved in this scheme grows linearly with the number of N of single electron states, whereas in the exact approach this number is essentially the number of molecular states $\sim 2^N$.

To illustrate the nature of the kinetics that results from these rate processes, we choose a set of physically reasonable parameters. In the calculation discussed below, the following choice was used: $\mu_L = 0.0$ eV, $\mu_R = \mu_L + |e|U$, $\varepsilon_{D1} = -0.1$ eV, $\varepsilon_{D2} = 1.4$ eV, $\varepsilon_{A2} = 0.9$ eV, $V_C = 0.25$ eV, and $V_C' = 0.15$ eV. Therefore, $\Delta E_D = \varepsilon_{D2} - \varepsilon_{D1} = 1.5$ eV[19] and $V_C + V_C' = 0.4$ eV.[20,21] For the temperatures we take $T = 300$ K and $T_s = 6000$ K. The kinetic rates are set to $\nu_L = \nu_R = \nu_S = \nu_{nr} = 0.01\nu_{DA}$ and $\nu_{DA} = 10^{12}$ s^{-1}, describing a system with efficient and fast donor-to-acceptor electron transfer (which can occur on the picosecond time scale[22]) and moderate radiationless losses, as would be used in such applications. Finally, note that in the particular example employed here we have considered a situation where the imposed potential bias falls between the acceptor species and the right electrode. It should be emphasized that although the results shown in Figures 3 and 4 are based on these choices, the qualitative behavior discussed below holds for a wide range of these parameters.

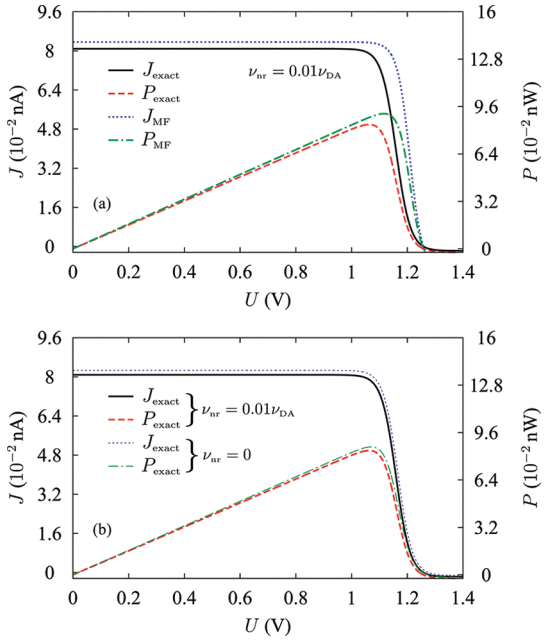

Figure 3. Current (J, left vertical axis) and power ($P = UJ$, right vertical axis) in the PV cell, plotted against the voltage bias U (see text for parameters). Plot (a) compares results from the exact calculation to those obtained from mean-field approximation. Plot (b) compares the same exact results ($\nu_{nr} = 0.01\nu_{DA}$) as those obtained for the ideal cell for which $\nu_{nr} = 0$. We assume that $\nu_{DA} = 10^{12}$ s^{-1}.

RESULTS AND DISCUSSIONS

Figure 3 shows results for the stationary donor → acceptor current obtained from both the exact solution from eqs 9−19 and the mean-field approximation, eqs 20−28. Figure 3a compares the results of the mean-field approach to their exact counterpart, showing that the former provides a good approximation to the exact behavior. Figure 3b compares the performance of a junction characterized by the prescribed parameters to the corresponding ideal junction in which nonradiative losses are absent ($\nu_{nr} = 0$). In both cases, the current is constant until the electrochemical potential on the right electrode comes within $\sim k_B T$ of the acceptor level A2 and decreases sharply after it exceeds this level. Consequently, the generated power, $P(U) = UJ(U)$, goes through a sharp maximum, $P_{max} = U_{max}J(U_{max})$, in that voltage region.

Next, consider the efficiency. The maximal power conversion efficiency is defined by

$$\eta = \frac{P_{max}}{P_S} = \frac{U_{max}J(U_{max})}{P_S} \tag{29}$$

where P_S is the incident radiant power, a constant independent of the process undergone by the system. The thermodynamic efficiency at maximum power is given by

$$\eta^* \equiv \frac{P_{max}}{\dot{Q}_S} = \frac{U_{max}J(U_{max})}{\Delta E_D J_S(U_{max})} = \frac{U_{max}}{\Delta E_D}\left(1 + \frac{J_{nr}(U_{max})}{J_S(U_{max})}\right) \tag{30}$$

dx.doi.org/10.1021/jp205856x |J. Phys. Chem. C 2011, 115, 21396–21401

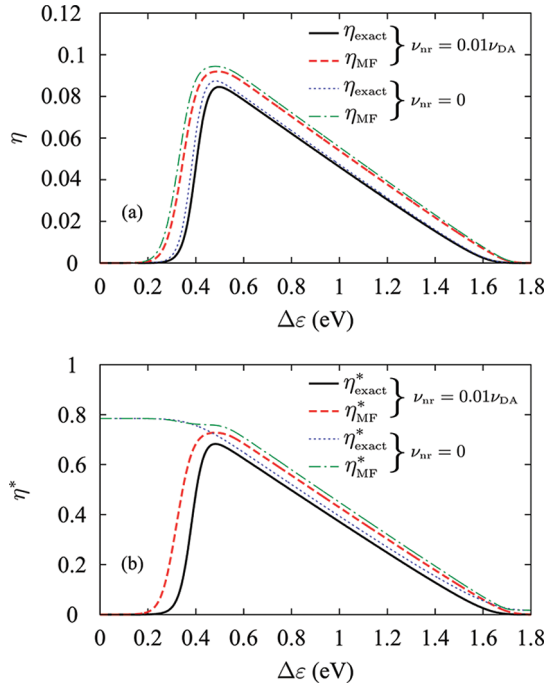

Figure 4. (a) Power conversion efficiency η and (b) thermodynamic efficiency η^* evaluated at maximum power and displayed as functions of the interface gap $\Delta\varepsilon$. Mean-field results are compared with the exact solutions of the underlying master equation. Parameters are the same as those in Figure 3 with the difference that ε_{A2} runs from 1.4 to −0.4 eV, and μ_R is determined by P_{max}. For the power, $P = P_S$ incident on the cell, we assume 1.0 nW.[24]

where $\dot{Q}_S$ is the net energy absorbed per unit time from the radiation field, that is, heat absorbed from the hot reservoir, $\dot{Q}_S = \Delta E_D J_S$. We note in passing that all processes undergone by our system are accompanied by well-defined energy changes: The heat fluxes associated with the electron exchange processes between system and leads, are, in the present model $\dot{Q}_L = (\varepsilon_{D1} - \mu_L)J_L$, $\dot{Q}_R = (\mu_R - \varepsilon_{A2})J_R$, and $\dot{Q}_{nr} = \Delta E_D J_{nr}$ is the net heat generation per unit time related to nonradiative relaxation processes, and $\dot{Q}_{DA} = -\Delta\varepsilon J_{DA}$ is the heat flux associated with the electron transfer at the D−A interface. Energy conservation implies that the overall cell power is the sum of these fluxes, that is, $P = \dot{Q}_L + \dot{Q}_R + \dot{Q}_S + \dot{Q}_{nr} + \dot{Q}_{DA} \equiv (\mu_R - \mu_L)J = UJ$.

Of central importance is the dependence of the efficiency on the interface LUMO−LUMO energy gap $\Delta\varepsilon$. One may intuitively expect to find that an optimal value of this parameter exists: A finite $\Delta\varepsilon$ is needed to drive the charge separation process, but a larger $\Delta\varepsilon$ implies that more energy may be lost to unproductive processes. Equations 29 and 30 quantify this phenomenon, which is illustrated in Figure 4. Figure 4a shows the power conversion efficiency calculated for the chosen parameter set using eq 29. For comparison, the corresponding result for the ideal cell ($\nu_{nr} = 0$) is also shown. Both are seen to go through a maximum as functions of the interfacial LUMO−LUMO gap $\Delta\varepsilon$. The thermodynamic efficiency, eq 30, displayed against $\Delta\varepsilon$ in Figure 4b shows a similar pronounced maximum; however, the ideal thermodynamic efficiency is a monotonously decreasing function of $\Delta\varepsilon$. Note that the ideal cell efficiency is an upper bound to the actual efficiency; however, for this finite power operation, it is below the Carnot efficiency, $\eta_C = 1 - T/T_S = 0.95$.

Finally, consider again the performance of the mean-field approximation relative to the exact solution. As seen from Figures 3 and 4, the mean-field treatment provides a good approximation that closely follows the behavior of exact solutions. The influence of correlations is particularly seen in Figure 4b, where we find small but noticeable differences between the mean-field and the exact curves for $\Delta\varepsilon$ beyond the maximum at ∼0.4 eV.

CONCLUSIONS

In summary, the effort to increase and optimize the efficiency of heterojunction OPVs necessarily involves many structural and energetics system parameters. The above considerations focus on what is arguably the most important generic issue — the optimization of the interfacial LUMO−LUMO gap that compensates between the need to overcome the exciton binding energy and the required minimization of losses. For the present simplified model and our choice of parameters, we find the most efficient setup for interface gap energies somewhat above 0.4 eV. More important is the fact that the present model, with future generalizations that should include transport in the donor and acceptor phases and polaronic relaxation following redistribution of charge densities, provides a framework for analyzing such efficiency measures. The mean-field approach introduced here provides a reliable approximation that can be used for fast evaluation of more complex model systems and will be useful in extending these studies to realistic OPV cell models. A more ambitious task would be to generalize the concept advanced in the Article to the quantum regime. Consideration of quantum effects and coherence (see, for example, ref 23) may prove useful in the discussion of fundamental limits to photovoltaic efficiency.

AUTHOR INFORMATION

Corresponding Author

*E-mail: meinax@uos.de; nitzan@post.tau.ac.il.

ACKNOWLEDGMENT

We thank Prof. Mark Ratner for helpful discussions. M.E. gratefully acknowledges funding by a Forschungsstipendium by the Deutsche Forschungsgemeinschaft (DFG, grant number EI 859/1-1). The research of A.N. is supported by the Israel Science Foundation, the Israel-US Binational Science Foundation, the European Science Council (FP7/ERC grant no. 226628), and the Israel - Niedersachsen Research Fund.

REFERENCES

(1) Deibel, C.; Dyakonov, V. *Rep. Prog. Phys.* **2010**, *73*, 096401.
(2) Nicholson, P. G.; Castro, F. A. *Nanotechnology* **2010**, *21*, 492001.
(3) Sariciftci, N. S.; Smilowitz, L.; Heeger, A. J.; Wudl, F. *Science* **1992**, *258*, 1474–1476.
(4) Yu, G.; Gao, J.; Hummelen, J. C.; Wudl, F.; Heeger, A. J. *Science* **1995**, *270*, 1789–1791.
(5) Hoppe, H.; Sariciftci, N. S. *J. Mater. Res.* **2004**, *19*, 1924–1945.
(6) Koeppe, R.; Sariciftci, N. S. *Photochem. Photobiol. Sci.* **2006**, *5*, 1122–1131.
(7) Rutten, B.; Esposito, M.; Cleuren, B. *Phys. Rev. B* **2009**, *80*, 235122.
(8) Giebink, N. C.; Wiederrecht, G. P.; Wasielewski, M. R.; Forrest, S. R. *Phys. Rev. B* **2011**, *83*, 195326.
(9) Potscavage, W. J.; Sharma, A.; Kippelen, B. *Acc. Chem. Res.* **2009**, *42*, 1758–1767.

(10) Einax, M.; Solomon, G. C.; Dieterich, W.; Nitzan, A. *J. Chem. Phys.* **2010**, *133*, 054102.
(11) Einax, M.; Körner, M.; Maass, P.; Nitzan, A. *Phys. Chem. Chem. Phys.* **2010**, *12*, 645–654.
(12) Dierl, M.; Maass, P.; Einax, M. *Europhys. Lett.* **2011**, *93*, 50003.
(13) Sylvester-Hvid, K. O.; Rettrup, S.; Ratner, M. A. *J. Phys. Chem. B* **2004**, *108*, 4296–4307.
(14) Nelson, J.; Kirkpatrick, J.; Ravirajan, P. *Phys. Rev. B* **2004**, *69*, 035337.
(15) Burlakov, V. M.; Kawata, K.; Assender, H. E.; Briggs, G. A. D.; Ruseckas, A.; Samuel, I. D. W. *Phys. Rev. B* **2005**, *72*, 075206.
(16) Lei, B.; Yao, Y.; Kumar, A.; Yang, Y.; Ozolins, V. *J. Appl. Phys.* **2008**, *104*, 024504.
(17) Wagenpfahl, A.; Deibel, C.; Dyakonov, V. *IEEE J. Sel. Top. Quantum Electron.* **2010**, *16*, 1759–1763.
(18) Arkhipov, V. I.; Emelianova, E. V.; Bässler, H. *Phys. Rev. Lett.* **1999**, *82*, 1321–1324.
(19) Soci, C.; Hwang, I.-W.; Moses, D.; Zhu, Z.; Waller, D.; Gaudiana, R.; Brabec, C. J.; Heeger, A. J. *Adv. Funct. Mater.* **2007**, *17*, 632–636.
(20) Gregg, B. A.; Hanna, M. C. *J. Appl. Phys.* **2003**, *93*, 3605–3614.
(21) Pensack, R. D.; Asbury, J. B. *J. Phys. Chem. Lett.* **2010**, *1*, 2255–2263.
(22) Rice, M. J.; Gartstein, Y. N. *Phys. Rev. B* **1996**, *53*, 10764–10770.
(23) Scully, M. O. *Phys. Rev. Lett.* **2010**, *104*, 207701.
(24) We take air mass 1.5 under standard test conditions (corresponds to 1000 Wm^{-2}) and assuming an illuminated area of 1 μm^2.